



HAL
open science

Solvothermal Vapor Annealing of Lamellar Poly(styrene)- block -poly(d , l -lactide) Block Copolymer Thin Films for Directed Self-Assembly Application

Cian Cummins, Parvaneh Mokarian-Tabari, Pascal Andrezza, Christophe Sinturel, Michael Morris

► To cite this version:

Cian Cummins, Parvaneh Mokarian-Tabari, Pascal Andrezza, Christophe Sinturel, Michael Morris. Solvothermal Vapor Annealing of Lamellar Poly(styrene)- block -poly(d , l -lactide) Block Copolymer Thin Films for Directed Self-Assembly Application. *ACS Applied Materials & Interfaces*, 2016, 8 (12), pp.8295-8304. 10.1021/acsami.6b00765 . hal-03614806

HAL Id: hal-03614806

<https://hal.science/hal-03614806>

Submitted on 19 Aug 2022

HAL is a multi-disciplinary open access archive for the deposit and dissemination of scientific research documents, whether they are published or not. The documents may come from teaching and research institutions in France or abroad, or from public or private research centers.

L'archive ouverte pluridisciplinaire **HAL**, est destinée au dépôt et à la diffusion de documents scientifiques de niveau recherche, publiés ou non, émanant des établissements d'enseignement et de recherche français ou étrangers, des laboratoires publics ou privés.

Solvo-thermal vapor annealing of lamellar poly(styrene)-*block*-poly(D,L-lactide) block copolymer thin films for directed self-assembly application

Cian Cummins,^{*,†,§} Parvaneh Mokarian-Tabari,^{*,†,§} Pascal Andrezza,[‡]
Christophe Sinturel,[‡] and Michael A. Morris^{†,§}

[†] Materials Research Group, Department of Chemistry and Tyndall National Institute, University College Cork, Cork, Ireland.

[‡] ICMN, UMR 7374 - CNRS / Université d'Orléans, 1b rue de la Férollerie, 45071 Orléans, France.

[§] AMBER@CRANN, Trinity College Dublin, Dublin, Ireland.

* **Corresponding author: cian.a.cummins@gmail.com, p.mokarian@ucc.ie**

ABSTRACT

Solvo-thermal vapor annealing (STVA) was employed to induce microphase separation in a lamellar forming block copolymer (BCP) thin film containing a readily degradable block. Directed self-assembly of poly(styrene)-*block*-poly(D,L-lactide) (PS-*b*-PLA) BCP films using topographically patterned silicon nitride was demonstrated with alignment over macroscopic areas. Interestingly, we observed lamellar patterns aligned parallel as well as perpendicular (perpendicular microdomains to substrate in both cases) to the topography of the graphoepitaxial guiding patterns. PS-*b*-PLA BCP microphase separated with high a degree of order in an atmosphere of tetrahydrofuran (THF) at an elevated vapor pressure (at ca. 40-60°C). Grazing incidence small angle X-ray scattering (GISAXS) measurements of PS-*b*-PLA films reveals the through-film uniformity of perpendicular microdomains after STVA. Perpendicular lamellar orientation was observed on both hydrophilic and relatively hydrophobic surfaces with a domain spacing (L_0) of ~ 32.5 nm. The rapid removal of the PLA microdomains is demonstrated using a mild basic solution for the development of a well-defined PS mask template. GISAXS data reveals the through-film uniformity is retained following wet etching. The experimental results in this article demonstrate highly oriented

1
2
3 PS-*b*-PLA microdomains after a short annealing period and facile PLA removal so as to form
4
5 porous on-chip etch masks for nanolithography application.
6
7

8 9 INTRODUCTION

10
11 Nanoscale patterning of thin films using BCP self-assembly is a facile (at least in principle)
12
13 and low cost route to form well-registered and highly defined domains of sizes from 3-100
14
15 nm.¹ Depending on the BCP composition, arrangements with spherical, cylindrical, gyroidal
16
17 and lamellar geometries can be developed over large areas. Desired morphology and length
18
19 scales can be achieved via variation of the volume fraction (f) of the blocks and through
20
21 tailoring of the BCP chain lengths, *i.e.* the degree of polymerization (N). Such complex yet
22
23 ordered microdomains provide an ideal platform for use in neuroprosthetic technologies,²
24
25 membrane/filtration systems,^{3,4} memory storage devices^{5,6,7} and photovoltaics.^{8,9} Another
26
27 potential application has focused on using BCP templates as on-chip etch masks for next-
28
29 generation lithography.¹⁰
30
31
32
33
34
35

36
37 Directed self-assembly (DSA) of BCPs is a promising candidate for augmenting the
38
39 lithographic patterning process to enable higher computing speed and reduced power
40
41 consumption per device function (*i.e.* Moore's Law).¹¹ Two key challenges in the BCP
42
43 nanolithography field include the placement and registration of features and the ability to
44
45 define ultra-small critical dimensions. Graphoepitaxy is used to obtain long range order and
46
47 alignment of BCP features via trenches lithographically defined prior to BCP deposition and
48
49 self-assembly.^{12,13,14,15,16} Similarly, chemoepitaxy developed by Nealey and co-workers
50
51 demonstrates extreme precision by using lithographically defined chemical patterns to control
52
53 PS-*b*-poly(methyl methacrylate, PMMA) assembly and alignment.^{17,18} Low line edge
54
55 roughness of resulting pattern transferred nanostructures, high areal density and ease of
56
57
58
59
60

1
2
3 processing (and similarity to industry patterning) are some of the main attributes that have led
4 to graphoepitaxy and chemoepitaxy being at the forefront of alternative patterning
5 methodologies. BCP material criteria beyond the “first generation” PS-*b*-PMMA include a
6 BCP possessing a high Flory-Huggins interaction parameter (*i.e.* χ)¹⁹ and high etch contrast
7 to allow sub-10 nm critical dimensions (CD) to be attained following pattern transfer. New
8 BCP materials possessing a high χ have been reported of late which can access sub-10 nm
9 feature sizes.^{20,21,22,23,24,25}

10
11
12
13
14
15
16
17
18
19
20 Shear force,²⁶ magnetic fields,²⁷ and thermal annealing²⁸ are routinely employed for the self-
21 assembly of BCP thin film morphologies. More recently, microwave irradiation was shown to
22 induce self-assembly in a range of high χ BCPs in sub-2 minute processes.^{29,30,31,32}
23 Controlling BCP microdomain orientation (*i.e.* direction to the surface plane) is paramount
24 for most chosen applications and solvent vapor annealing (SVA) has been utilized to induce
25 self-assembly and manipulate microdomain orientation.³³ SVA is a technique that plasticizes
26 polymer material and the solvent-polymer interaction reduces the diffusive energy barrier
27 promoting microphase separation at lower temperatures.³⁴ Despite its widespread use the
28 interpretation and exact mechanism(s) of the SVA method are not fully understood. Various
29 mechanisms have been postulated from empirical evidence. Gu *et al.*^{35,36} have recently
30 provided an insight on poly(styrene)-*block*-poly(2-vinylpyridine) (PS-*b*-P2VP) BCPs and
31 highlight the importance of taking into account the processing conditions such as the swelling
32 ratio of BCP films and solvent removal rates during SVA. The work by Gu *et al.* further
33 emphasizes the benefits of grazing incidence small angle X-ray scattering (GISAXS) as a
34 characterization method that has also been carried out on other BCP systems regarding
35 swelling effects.^{37,38} Likewise, Mokarian *et al.*³⁹ employed an *in-situ* time-resolved light
36 scattering device to observe a “flipping” phenomenon in cylindrical forming PS-*block*-
37
38
39
40
41
42
43
44
45
46
47
48
49
50
51
52
53
54
55
56
57
58
59
60

1
2
3 poly(ethylene oxide) (PS-*b*-PEO) films that was related to vapor pressure threshold value. In
4
5 addition to using a solvent to impart mobility in a BCP, combining the solvent vapors with
6
7 temperature (solvo-thermal vapor annealing, STVA) to increase vapor pressure also enhances
8
9 the ordering dynamics of BCPs.^{34,40} The complex interplay of surface energetics and
10
11 confinement effects of BCPs in thin film form requires extensive solvent analysis. Each
12
13 polymer block swells at different rates depending on the selectivity of the exposed solvent.
14
15 The affinity of the two blocks is dynamic in nature and can be affected by solvent uptake as
16
17 defined by equation 1 below.^{39,41}
18
19

$$\chi_{\text{eff}} = \chi(1 - \Phi_s) \quad (1)$$

20
21
22
23
24
25
26
27 where χ_{eff} and χ are the Flory-Huggins interaction parameters in the presence and absence of
28
29 the solvent respectively. The parameter Φ_s is the volume fraction of solvent. From equation
30
31 1, solvent uptake by the polymer film will reduce the overall χ of the system, however,
32
33 solvent use is required to reduce the glass transition of the PS block enabling microphase
34
35 separation.⁴¹ Lamellar PS-*b*-PLA studies to date have focused mainly on thermal
36
37 annealing.^{42,43} Keen *et al.*⁴³ have demonstrated DSA of PS-*b*-PLA with sub-10 nm feature
38
39 sizes and outlined key contributions on the relationship between defect levels and degree of
40
41 frustration of polymer chains under confinement.
42
43
44

45
46
47 We present a systematic study using atomic force microscopy data complemented by
48
49 GISAXS analysis on the STVA behavior and microphase separation of a near symmetric
50
51 forming PS-*b*-PLA BCP thin film. The work highlights key experimental parameters in SVA
52
53 practices to achieve excellent microphase separation in a lamellar PS-*b*-PLA system. We
54
55 show through STVA the microphase separation of PS-*b*-PLA (21 kg mol⁻¹ – 19 kg mol⁻¹)
56
57
58
59
60

1
2
3 BCP system and the DSA of line patterns on topographically patterned silicon nitride
4 substrates. GISAXS provided an interesting insight on the interior orientation of the PS-*b*-
5 PLA films following STVA. Our studies showed that microphase separated BCP patterns
6
7
8
9
10 were attained only through increasing THF vapor pressure using a higher processing
11
12 temperature. Wet etching of the PLA component in PS-*b*-PLA films is also detailed showing
13
14 a high degree of selectivity.
15
16
17

18 EXPERIMENTAL

20
21 **Materials.** Polystyrene-*block*-polylactide (referred to as PS-*b*-PLA, but note that PLA is in
22 the DL form) was purchased from Polymer Source, Inc., Canada, with a total number average
23 molecular weight of $M_n = 40.5 \text{ kg mol}^{-1}$ ($M_{nPS} = 21 \text{ kg mol}^{-1}$; $M_{nPLA} = 19.5 \text{ kg mol}^{-1}$, $f_{PS} =$
24 0.53), a polydispersity index of 1.15 and was used without further purification or treatment.
25
26
27 The planar substrates used were highly polished single-crystal silicon <100> wafers (p-type)
28
29 with a native oxide layer of 2 nm. The silicon nitride (Si_3N_4) substrates were Si_3N_4 coated
30
31 silicon wafers (p-type silicon <100> with a surface SiO_2 layer $\sim 7 \text{ nm}$ thick) using a low
32
33 pressure chemical vapor deposition method and had a resistivity, ρ , = 1×10^{14} to $1 \times 10^{16} \Omega$
34
35 cm. Topographically patterned Si_3N_4 substrates with pitches in the range of 50–500 nm,
36
37
38 variable mesa widths of 30–700 nm and depth of ~ 50 –60 nm were fabricated via 193 nm UV-
39
40 lithography and processed by means of conventional mask and etch techniques. SEM and
41
42 TEM characterization of the Si_3N_4 substrates can be found elsewhere.³¹ Sulfuric acid (ACS
43
44 reagent, 95.0-98.0%), hydrogen peroxide (containing inhibitor, 30 wt. % in H_2O , ACS
45
46 reagent), methanol (for HPLC, $\geq 99.9\%$) chloroform (HPLC grade, $\geq 99.9\%$, contains 0.5–
47
48 1.0% ethanol as stabilizer,), toluene (for HPLC, 99.9%), tetrahydrofuran (THF) (HPLC
49
50 grade, $\geq 99.9\%$), hexamethyldisilazane, sodium hydroxide (purum p.a., $\geq 98.0\%$ (T), beads),
51
52
53
54
55
56
57
58
59
60

1
2
3 ruthenium(III) chloride hydrate, and sodium hypochlorite solution (6-14% active chlorine
4 basis) were all purchased from Sigma Aldrich.
5
6

7 **Substrate Cleaning, Block Copolymer Preparation and Deposition.** Substrates were cut
8 into 2.0 cm² pieces and were cleaned in a piranha solution (1 : 3 v/v 30% H₂O₂ : H₂SO₄)
9 (Caution – piranha solution may cause explosion in contact with organic material) at 100°C
10 for 30 minutes, rinsed with DI waters several times and dried using nitrogen gas. Following
11 this, the freshly piranha cleaned substrates were sonicated with chloroform (*i.e.* BCP casting
12 solvent) for 10 minutes. Substrates that were functionalized with a hexamethyldisilazane
13 (HMDS) layer were first sonicated with acetone followed by methanol (20 minutes sonication
14 in each). After sonication, the substrates were immersed in a solution of toluene:HMDS (1:5)
15 for ~16 h, as described previously in the literature.⁴⁴ 0.5 wt % solutions of PS-*b*-PLA were
16 prepared in chloroform and subsequently sonicated for 30 minutes. Following complete
17 dissolution, PS-*b*-PLA solution was spin coated on piranha cleaned silicon substrates at 2000
18 rpm for 30 seconds. 0.5 wt % PS-*b*-PLA solutions were spin coated on HMDS treated silicon
19 in the same manner. Note that the HMDS step was carried out so that film delamination was
20 avoided via promotion of PS adhesion onto the HMDS functionalized substrate. Following
21 PS-*b*-PLA deposition, solvent vapor annealing (SVA) treatment was carried out. Films were
22 placed inside a glass jar (150 ml) with a small vial containing ~1 ml of THF solvent for up to
23 60 minutes. This was the standard protocol for all temperatures; room temperature, 40°C and
24 55°C were examined. Note in this work, we make a distinction between SVA, *i.e.* room
25 temperature solvent vapor annealing and STVA, *i.e.* solvent vapor annealing with
26 temperature. Prior to SVA films at room temperature, the vial containing THF solvent was
27 placed inside the annealing jar for up to 20 minutes before sample to ensure a saturated THF
28 atmosphere was reached. Following the desired SVA or STVA period, the film was removed
29
30
31
32
33
34
35
36
37
38
39
40
41
42
43
44
45
46
47
48
49
50
51
52
53
54
55
56
57
58
59
60

1
2
3 immediately and solvent was allowed to evaporate at ambient conditions before
4
5 characterization.
6

7 **Grazing Incidence Small Angle X-Ray Scattering (GISAXS).** The experiments were
8
9 performed on the “Xeuss” Xenocs X-ray scattering set-up with a monochromatic x-ray beam
10
11 at 8040 eV. X-ray scattering measurements geometry is defined by the direct beam incidence
12
13 α_i and the scattered intensity as a function of the out-of-plane angle α_f with respect to the
14
15 substrate surface and of the in-plane angle δ . The components of the wavevector transfer
16
17 (transferred momentum) $q = k_i - k_f$, defined by the incident k_i and the scattered k_f wave
18
19 vectors are defined in the laboratory frame, as x and y in the surface substrate plane and z
20
21 out-of plane (y perpendicular to the incident beam).^{45,46,47,48} To enhance the scattering signal
22
23 coming from the polymer film surface, the X-ray grazing incidence angle of 0.22° was
24
25 selected above the critical angle of the film, probing inside the film and just at the critical
26
27 angle of silicon substrate. The two-dimensional GISAXS pattern was recorded using a high
28
29 sensitivity 2D detection (Pilatus 300K hybrid pixel) placed at a distance of 2520 mm from the
30
31 sample, perpendicular to the x axis. The scattered beam intensities were collected, in a range
32
33 between $[0; 2.5\text{nm}^{-1}]$, by averaging ten frames to improve the counting statistic. To extract
34
35 morphological information, data analyses are realized on two sections of the 2D patterns. The
36
37 q_y (resp. q_z) section corresponds to the scattering signal along the direction parallel (resp.
38
39 perpendicular) to the substrate surface (Figure 2e). From these 1D cut, the contribution of the
40
41 form factor could be measured over the whole 2D pattern whereas the interference function,
42
43 which describes a simple in-plane correlation as well as a long range order^{47,49,50} is
44
45 observable only in the q_y direction.
46
47
48
49
50

51 **PLA block degradation/etch.** A 0.01M NaOH (60:40, water:methanol) solution was
52
53 prepared at room temperature. The solution was given sufficient time (~15 minutes) in order
54
55 to fully dissolve. STVA PS-*b*-PLA films were then immersed in the basic solution for up to 5
56
57
58
59
60

1
2
3 minutes. After removal from the degradation solution, films were washed twice with
4
5 deionized water and blown dry under nitrogen. Note we have previously investigated thicker
6
7 PS-*b*-PLA films (~ 200 nm) formed via “solvo-microwave” annealing that suffered from
8
9 pattern collapse upon wet etching.⁵¹ Therefore, thinner (< 50 nm) PS-*b*-PLA films were
10
11 evaluated in this work to overcome pattern collapse issues with a view to their
12
13 nanolithographic application.
14

15
16 **Characterization. Film Thickness.** BCP film thicknesses were measured with a
17
18 spectroscopic ellipsometer “J.A. Woollam Ellipsometer” at a fixed angle of incidence of 70°,
19
20 on at least five different places on the sample and was averaged as the film thickness. A layer
21
22 model (SiO₂ + BCP) for the total BCP film was used to simulate experimental data. **Atomic**
23
24 **Force Microscopy (AFM).** AFM (Park systems, XE-100) was operated in AC (tapping)
25
26 mode under ambient conditions using silicon microcantilever probe tips with a force constant
27
28 of 42 N m⁻¹. Topographic and phase images were recorded simultaneously. **Scanning**
29
30 **Electron Microscopy (SEM).** SEM images were obtained by a FEI Helios Nanolab 600i
31
32 system at an accelerating voltage of 5 kV and at a working distance of 4 mm. Cross-section
33
34 SEM images involved cleaving the substrate in half and positioning the substrate
35
36 perpendicular to the incident beam of electrons. The stage was then tilted at 20° to 30°.
37
38 **Fourier Transform-Infrared (FT-IR) Spectroscopy.** An IR660, Varian infrared
39
40 spectrometer was used to record the FT-IR spectra. The FT-IR was operated in attenuated
41
42 total reflection mode during measurements. The measurements were performed in the
43
44 spectral range of 4000 to 400 cm⁻¹, with a resolution of 1 cm⁻¹ and data averaged over 32
45
46 scans. FT-IR was employed to analyze films before and after etching the PLA block of the
47
48 PS-*b*-PLA BCP.
49
50
51
52

53 54 55 56 **RESULTS AND DISCUSSION** 57 58 59 60

Microphase separation of PS-*b*-PLA BCP

Our investigation examined PS-*b*-PLA films over a range of temperatures while exposed to solvent vapors. Films were separately exposed to either a polar (THF) or non-polar solvent (CHCl₃) vapor at room temperature and at 40°C, and at 55°C to increase the solvent vapor pressure in an attempt to achieve microphase separation via enhanced chain mobility. During the SVA process of BCP films, free volume is created in the polymer network which decreases the glass transition temperature (T_g) of the polymer and, thus, enhances chain mobility. Solubility parameters for PS, PLA and THF are 18.8, 22.2 and 19.4 [MPa]^{1/2} respectively.^{52,53,54} Thin films of PS-*b*-PLA were initially prepared on silicon substrates following piranha cleaning. AFM topographic images of 0.5 wt % PS-*b*-PLA thin films are shown in Figure 1 (a and b) after 30 min and 45 min exposure to THF vapor at room temperature, 40°C and 55°C. THF is a relatively neutral solvent for both PS and PLA blocks (see Table 1) and was employed as our SVA solvent. One observes poor microphase separated features at room temperature at 30 min and 45 min exposure, however well-ordered “fingerprint” patterns are seen at higher annealing temperatures. Distinct lamellar (as confirmed by GISAXS) patterns are consistently formed after 45 min STVA with THF vapor at 40°C (Figure 1d) and 55°C (Figure 1f). We also investigated chloroform as a SVA solvent as this was used as the spin casting solvent. Table 1 outlines the polymer-solvent interaction for THF and CHCl₃ at respective treatment temperatures and calculation are described in SI. Despite CHCl₃ possessing similar polymer-solvent interaction values to THF, microphase separation was not observed in the process window studied for CHCl₃ SVA (see SI Figure S1). Likewise, self-assembly was not observed for films that were thermally annealed at 40°C or at 55°C (see SI Figure S2).

1
2
3 We believe the neutral interface created at the polymer/air interface under STVA in THF
4
5 allows perpendicular orientation of the lamellar microdomains as others have also noted in
6
7 their experiments for similar systems.^{55,56} This neutral top layer ordains the orientation rather
8
9 than the substrate surface. GISAXS can be used to look for through-film structures as a result
10
11 of the possible “frustration” between any preferred orientation and/or segregation at the air
12
13 and substrate interfaces.
14
15

16
17
18 In order to understand the dynamics of ordering we carried out *ex-situ* GISAXS analysis on
19
20 PS-*b*-PLA thin films from their as-cast form to fully developed “fingerprint” features when
21
22 STVA at 55°C. The as-cast film of 0.5 wt% PS-*b*-PLA CHCl₃ solution spun onto silicon is
23
24 shown in Figure 2 (a). A near featureless film is observed. The initial as-cast film thickness
25
26 was measured at 47 nm. Samples STVA in THF vapor for 15 and 45 min at 55°C are shown
27
28 in Figure 2 (b) and (c). One can see that ordered self-assembly begins to occur after 15 min
29
30 and that fully developed domain structures with extended average line lengths are observed
31
32 after 45 min STVA. The perpendicular domains in Figure 2 (c) have a 32.5 nm periodicity
33
34 (L_0). After swelling of the film for 45 min with THF vapor at 55°C (Figure 2c), the dried film
35
36 thickness was, within experimental error, the same as the as-cast film at 48 nm \pm 0.5 nm.
37
38 Table 2 displays thicknesses for as-cast and STVA annealed films on piranha cleaned and
39
40 HMDS functionalized silicon substrates.
41
42
43
44
45

46
47 As time proceeds, we then observe a decrease in microdomain pitch but enhanced average
48
49 line lengths, see Figure 2 (a) – (c), as might be expected with the removal of solvent and the
50
51 film reaching a metastable state. We observed a notable difference between microdomain
52
53 pitches at 15 min STVA (38 \pm 0.2 nm) whilst 45 min STVA samples possessed a pitch of
54
55 32.5 \pm 0.2 nm. The through film uniformity, an essential feature of block polymer etch masks
56
57
58
59
60

1
2
3 for nanolithography, observed for Figure 2 (c) is also confirmed by GISAXS analysis. One
4
5 could also claim that the morphologies achieved in the swollen state during STVA have been
6
7 retained upon evaporation (dry state) as from AFM data they are quite distinct from the as-
8
9 cast to the morphologies observed after particular annealing times. A similar work has
10
11 recently been shown and analyzed for asymmetric PS-*b*-PLA system by Sinturel *et al.*³⁸
12
13

14
15
16 Detailed GISAXS analysis was carried out on the above STVA films displayed in Figure 2
17
18 (a)-(c). The GISAXS patterns reveal that the scattering intensity is dominated by the
19
20 interference function in the q_y direction, whereas the contribution of the form factor is mainly
21
22 observable along the q_z direction. The as-cast, 15 minute and 45 minute treated films
23
24 exhibited a correlation peak with at least one order as seen in GISAXS patterns in Figure 2
25
26 (e), (f) and (g). One observes a large disorder in the as-cast film shown in Figure 2 (d) in the
27
28 in-plane correlation which is consistent with AFM image in Figure 2 (a). Using the distorted-
29
30 wave Born approximation (DWBA),⁵⁷ simulations of the intensities in the q_y (resp. q_z) in-
31
32 plane (resp. out-of-plane) direction are shown in Figure 3 (a) and (b) with a good adjustment
33
34 with the experimental cross sections. The fitting parameters reveal a large distance
35
36 distribution of the domains ($L_0 = 27 \pm 7$ nm) with a limited height 5-10 nm, not in the entire
37
38 thickness of the film but randomly dispersed in the film. GISAXS data of the PS-*b*-PLA film
39
40 from Figure 2 (b and c) are displayed in Figure 2 (e and f respectively) showing a well-
41
42 ordered correlation within the plane of the substrate in comparison to the poor correlation
43
44 observed in Figure 2 (d). The first order and third order peaks are observed only. The
45
46 extinction of such orders (second order) is due to the form factor of the lamellar domains (w
47
48 width, l length).⁵⁸ This effect is stronger in the sample STVA with THF for 45 min: the low
49
50 width dispersity (expected in self-assembled BCP) induced a series of intensity minima
51
52 which extinct the first pair orders of the interference peaks. Figure 3 (c) and (d) show the in-
53
54
55
56
57
58
59
60

1
2
3 plane simulation taking into account this effect with a width to interdistance ratio $w/L_0 = 2/3$
4
5 ($w = 22\text{nm}$). The simulation parameters reveal the local order of the lamellar organization
6
7 and the in-plane orientation distribution in agreement with the AFM image (Figure 2(c)). The
8
9 average local aspect ratio is around 5 (length/width) corresponding to the maximum value of
10
11 the coherence length of the measurement.
12
13

14 15 16 **Directed Self-Assembly of PS-*b*-PLA Via Topographic Substrates.**

17
18 For BCP materials to realize their nanolithographic potential, integration with top-down
19
20 lithographically patterned substrates must be demonstrated.¹¹ We have employed Si_3N_4
21
22 trenched substrates (see experimental for fabrication details) to graphoepitaxially align PS-*b*-
23
24 PLA films. Note that the use of “orientation” below refers to PS and PLA microdomains
25
26 relative to the substrate plane whilst “alignment” is in reference to the features relative to the
27
28 guiding sidewall geometry. Results presented in Figure 4 below were processed under the
29
30 same experimental parameters, *i.e.* film thickness (48 nm), STVA time and temperature (45
31
32 min @ 55°C). Figure 4 (a) reveals a large area of perpendicular alignment of PS-*b*-PLA
33
34 features to the Si_3N_4 guiding sidewalls. The channel dimensions (dark) in Figure 4 (a) and (b)
35
36 are $\sim 50\text{ nm}$ ($1.53 L_0$) wide while the mesa dimensions (bright) are $\sim 140\text{ nm}$. L_0 measured in
37
38 the channels is similar as that measured on planar silicon and open areas of the Si_3N_4
39
40 substrates at $\sim 32.5\text{ nm}$. The perpendicular alignment preference of the microdomains to the
41
42 sidewalls is also revealed in Figure 4 (c) with channel width dimensions slightly wider at \sim
43
44 100 nm ($\sim 3.08 L_0$) with mesa dimensions at $\sim 210\text{ nm}$ respectively.
45
46
47
48
49

50
51 This orientation of the microdomains is due to the neutral sidewalls. Additionally, despite
52
53 channel widths ranging from $\sim 50\text{ nm}$ to $\sim 100\text{ nm}$ the perpendicular orientation is retained.
54
55 We assume that the neutrality of the graphoepitaxy sidewalls favor a perpendicular
56
57
58
59
60

1
2
3 registration although this evolution of orientation is surprising in comparison to
4 graphoepitaxial alignment in general. However, if one compares the near identical surface
5 energies of the constituent blocks, $\gamma^{\text{PS}} = 42 \text{ mJ m}^{-2}$ and $\gamma^{\text{PLA}} = 36.0\text{--}41.1 \text{ mJ m}^{-2}$,^{32,42} the
6 perpendicular alignment to guiding features may be expected as neither block has a wetting
7 preference. Other reports have shown similar alignment results in graphoepitaxy schemes and
8 were described as resulting from a result of surface chemistry interactions,⁵⁹ solvent anneal
9 conditions,⁶⁰ mesa widths⁶⁰ or film thickness.⁶¹ In this work, it appears that the neutral
10 sidewalls and confinement of PS-*b*-PLA material favors perpendicular alignment. Also, it is
11 possible that PS and PLA microdomains are oriented parallel to the substrate surface on the
12 mesas and we cannot observe patterns by SEM. However, this seems less likely given the
13 work described above on planar substrates.

14
15
16
17
18
19
20
21
22
23
24
25
26
27 A further evolution of alignment direction of PS and PLA microdomains to sidewall features
28 was also observed. Figure 4 (d) – (f) show different channel (trench) and mesa dimensions
29 that produced parallel alignment to sidewalls for the PS-*b*-PLA films over macroscopic areas.
30 Notably, the area shows PS-*b*-PLA material that aligned parallel to channel sidewalls. The
31 channels (~140-200 nm, *i.e.* $4.3 > L_0 < 6.15$) in Figure 4 (d) – (f) are slightly wider than those
32 displayed in Figure 4 (a)-(c).

33
34
35
36
37
38
39
40
41
42
43 The reason for the change in pattern alignment is somewhat unexpected since surface
44 neutrality has not changed. We believe this observation is a manifestation of the effect of
45 entropy at the sidewall. Since we have not used a neutral brush and also there will be changes
46 in surface chemistry due to ambient exposure, it is highly unlikely that the surfaces are
47 ideally neutral and one block should be favoured at the substrate. However, the perpendicular
48 arrangement is caused because this arrangement increases entropy close to the sidewall. This
49 was first suggested by Pickett *et al.*⁶² and arises from chain end stretching. It is more
50
51
52
53
54
55
56
57
58
59
60

1
2
3 favourable at lower molecular weights and diminishes with distance from the wall. Thus, we
4
5 suggest this effect dominates at low pitch sizes but at the large channel widths, the parallel (to
6
7 the sidewall) arrangement is favored. Alternatively, it is plausible that the overflow of PS-*b*-
8
9 PLA has resulted in the alignment change of microdomains as depicted schematically in
10
11 Figure 4. We believe this is less likely as it relies on strong edge effects.
12
13

14
15
16 The graphoepitaxy process for both parallel and perpendicular alignment produces almost
17
18 defect-free patterns over large areas. However, further study is required to allow control of
19
20 the alignment direction of PS-*b*-PLA relative to guiding features. The use of polymer brushes
21
22 at channel bases or sidewalls as used for BCPs with similar block surface energies such as
23
24 PS-*b*-PMMA may be necessary for lamellar PS-*b*-PLA BCP.⁶³ Analyzing influencing
25
26 parameters such as film thickness, channel depths, and commensurability is also critical for
27
28 future work.
29
30
31

32 33 34 **Contributing factors to fast self-assembly of lamellar PS-*b*-PLA**

35
36 A number of factors contribute to the self-assembly of this PS-*b*-PLA system and the
37
38 organized features observed. Firstly, the PS-*b*-PLA diblock copolymer possesses a high χ (χ
39
40 @ 55°C ~ 0.187). The χ value for PS-*b*-PLA here is over four times higher than the well-
41
42 studied PS-*b*-PMMA (χ ~ 0.043 at 25°C) system. The Flory-Huggins interaction parameter
43
44 (χ) for PS-*b*-PLA was determined from equation 2 below which was previously established
45
46 experimentally;⁶⁴
47
48

$$49 \quad \chi(T) = (98.1) T^{-1} - 0.112 \quad (2)$$

50
51 where T represents absolute temperature. Additionally, after determining χ at the different
52
53 process temperatures employed here (see table 3), the corresponding χN values were
54
55 calculated. $\chi N > 10.495$ is the minimum threshold figure for microphase separation to occur
56
57
58
59
60

1
2
3 in BCP films.⁶⁵ The PS-*b*-PLA BCP used here has a χN value of 91.57, 84.06 and 78.20 at
4
5 23°C, 40°C, and 55°C respectively. These χN values are well above the minimum threshold
6
7 and are in the strong-segregation regime.⁶⁵
8
9

10
11 As mentioned above, an inherent property of the PS-*b*-PLA system is the similar surface
12
13 energies of the constituent PS and PLA blocks. PS-*b*-PLA is one of the few BCPs that exhibit
14
15 non-preferential free surface interactions. Neutralization of the free surface has been
16
17 established of late by Willson, Ellison and co-workers across a range of high χ silicon
18
19 containing BCPs with low pitch.^{21,24} Considering these contributing interfacial phenomena,
20
21 one can assume that a relatively neutral substrate/polymer interface combined with a
22
23 neutralized free surface for a lamellar PS-*b*-PLA will lead to perpendicular orientation of the
24
25 lamella domains.⁵⁶ Since the surface energies of PS-*b*-PLA allow a neutral substrate polymer
26
27 interface, controlling the polymer/air interface can be established via neutral SVA. As we
28
29 have demonstrated, THF exposure provides a neutralized free interface to enable highly
30
31 defined lamellar domains to orient perpendicular to the substrate surface. This is observed
32
33 from the highly developed PS-*b*-PLA domains seen in figure 2 (c) described above.
34
35
36
37
38
39

40
41 Figure 5 displays a graph of increasing THF vapor pressure due to increasing temperature.
42
43 THF vapor pressure was calculated using the Antoine equation (equation 3) where A, B, and
44
45 C are Antoine constants and for $23 < T < 100$ °C, A = 6.99, B = 1202.29, and C =
46
47 226.254.^{32,66}
48

$$P = 10^A - \left[\frac{B}{C+T} \right] \quad (3)$$

49
50
51
52
53
54 The insets (a-c) in Figure 5 show surface structures following SVA and STVA with THF at
55
56 room temperature (*i.e.* 23°C), 40°C and 55°C for 45 min. We believe that employing
57
58
59
60

1
2
3 temperature while SVA with THF for this particular PS-*b*-PLA system enables and enhances
4
5 microphase segregation for two reasons. Firstly, the increased vapor pressure allows a greater
6
7 concentration of THF molecules within the polymer network and for swelling to be affected
8
9 more rapidly than at room temperature. PS-*b*-PLA films exposed to THF vapor at room
10
11 temperature (THF nominal vapor pressure = 19.79 kPa) showed no distinct microphase
12
13 separation while films SVA at 40°C (THF nominal vapor pressure = 40.22 kPa) and 55°C
14
15 (THF nominal vapor pressure = 70.03 kPa) revealed well-defined domains. The importance
16
17 of vapor pressure and ability to enhance the dynamics of self-assembly has been highlighted
18
19 by our group for this system previously using “solvo-microwave” annealing.³² Secondly, as is
20
21 well demonstrated, thermal annealing alone enables the microphase separation of BCPs
22
23 above the T_g . Considering that exposure of polymer films to solvent vapor lowers the T_g of
24
25 BCP systems, the simultaneous treatment of a THF vaporized PS-*b*-PLA film even at low
26
27 temperatures should be sufficient for reorganization of polymer chains. We speculate that this
28
29 is the primary reason for observing such well-defined domains at 40°C. The T_g of PS and
30
31 PLA in this system is reported as 98°C and 49°C respectively from the supplier (see
32
33 experimental for further details). Solvent exposure using a miscible solvent combined with a
34
35 temperature (40°C) below the reported T_g provides more mobility to the PS and PLA block.
36
37
38
39
40
41
42

43 **PLA block removal forming PS mask template**

44
45 We have previously speculated the existence of a PLA wetting layer at the polymer/substrate
46
47 interface with this PS-*b*-PLA BCP system that leads to delamination of the film during wet
48
49 etching.⁵¹ It may be present due to the polar interaction of the PLA block and the native oxide
50
51 layer on silicon.⁶⁷ To overcome the wetting layer formation that leads to delamination of the
52
53 film, PS-OH brush or HMDS functionalization allows for wet etching to be carried out
54
55 without delamination of the polymer film.^{44,51} To demonstrate the delamination of a PS-*b*-
56
57
58
59
60

1
2
3 PLA film on a non-brush substrate we used a film with thickness close to ~ 210 nm so that a
4
5 color change or detachment of the polymer film could be easily observed by naked eye
6
7 following a brief etch in a 0.01M NaOH solution. The picture of the original self-assembled 2
8
9 wt % film is shown in SI Figure S3. SI Figure S3b shows the same film following etching in
10
11 a 0.5 M sodium hydroxide solution at room temperature. One observes a drastic color change
12
13 due to the loss of the polymer film. This simple observation shows that lamellar PS-*b*-PLA
14
15 films are susceptible to delamination owing to the PLA wetting layer at the polymer-substrate
16
17 interface. We carried out the same experiment after spin coating a 2 wt % PS-*b*-PLA solution
18
19 on a HMDS functionalized substrate. It should be noted the microphase separation is not
20
21 affected greatly when using the modified surface as shown in Figure 6a for 0.5 wt % PS-*b*-
22
23 PLA on HMDS silicon. Interestingly, we observed complete detachment of the PS
24
25 homopolymer film from the piranha cleaned silicon following etching. This shows that PS-*b*-
26
27 PLA BCP on piranha cleaned silicon may not solely be due to a PLA wetting layer but weak
28
29 PS interactions. Therefore, a HMDS functionalization step results in increased adherence and
30
31 thus enables wet etching of the PS-*b*-PLA BCP to be carried out.
32
33
34
35
36
37

38 For effective PLA etching, a 0.5 wt % PS-*b*-PLA film on a HMDS modified silicon substrate
39
40 was etched using a 0.01M sodium hydroxide solution for 5 min. From our previous work, we
41
42 have evaluated different routes and established issues that required further examination.⁵¹
43
44 Previously, we discussed that thinner block polymer films would be examined and this has
45
46 been demonstrated here. Figure 6a reveals well-developed microphase separated PS-*b*-PLA
47
48 pattern on HMDS functionalized silicon following SVA with THF at 55°C for 45 min.
49
50 Etching with 0.01M NaOH solution enabled porous PS templates after 5 min. Figure 6b
51
52 shows cross-section SEM image of PS soft mask template after PLA removal via wet etching.
53
54 The image shows that PS-fin collapse after PLA removal is not evident and reveals the high
55
56
57
58
59
60

1
2
3 selectivity of the etch and its' homogeneity over the film surface. The use of a low
4
5 concentration basic solution for PLA must be noted to avoid roughness. Over-etching is facile
6
7 with this system as the carboxylic acid backbone of the PLA block is susceptible to chain
8
9 scission.
10

11
12
13
14 Moreover, after the initial chain scission, auto-catalytic effects accelerate the degradation
15
16 process. The low concentration and short treatment time enabled effective PLA removal
17
18 without any damage to the overall structure. Etching a thin BCP film also avoids line collapse
19
20 that can occur due to the high aspect ratio of one microdomain relative to the other
21
22 microdomain (s) being removed.⁵¹ Such a scenario in thick films generally results in
23
24 collapsing of the remaining domains and merging of features. The GISAXS inset also shows
25
26 that the highly ordered vertical nature of the microdomains is retained, similar to initial PS-*b*-
27
28 PLA film. FT-IR data provided in Figure 6c confirms that PLA has been fully etched. The
29
30 characteristic C=O peak occurring at 1758 cm⁻¹ for the PLA backbone is present in the
31
32 unetched film while the after etch film (5 min in 0.01M NaOH solution) shows the absence of
33
34 this feature.
35
36
37
38
39

40 CONCLUSIONS

41
42 This article outlined a methodology using the solvo-thermal vapor annealing process for the
43
44 microphase separation of a symmetric PS-*b*-PLA BCP in a short processing period. Key
45
46 parameters influencing the self-assembly kinetics were examined and GISAXS data
47
48 confirmed that uniform films with high order and through film uniformity were formed after
49
50 optimum annealing. The PS-*b*-PLA BCP thin films developed in this work are of low aspect
51
52 ratio avoiding line collapse and image quality issues in order to optimize their
53
54 nanolithographic potential in DSA efforts. For pattern transfer purposes, we have also
55
56
57
58
59
60

1
2
3 demonstrated a highly PLA selective wet etch that can be carried out in a rapid, cheap and
4
5 reproducible manner. Additionally, DSA of line space features were shown with few defects
6
7 over large areas. The work presented here illustrates the applicability of a high χ BCP with a
8
9 rapidly degradable block for high etch contrast. However, careful substrate surface
10
11 modifications will be required to controllably align PS-*b*-PLA microdomains to a surface
12
13 plane to meet DSA requirements.
14
15

16 17 AUTHOR INFORMATION

18 19 Corresponding Author

20 * Cian Cummins: cian.a.cummins@gmail.com

21 * Parvaneh Mokarian-Tabari: p.mokarian@ucc.ie
22
23

24 25 Author Contributions

26 The manuscript was written through contributions of all authors. All authors have given
27 approval to the final version of the manuscript.
28
29

30 31 Notes

32 The authors declare no competing financial interest.
33
34
35
36
37

38 39 ACKNOWLEDGMENTS

40 The authors gratefully acknowledge financial support from AMBER Science Foundation
41 Ireland Center Grant (Grant number 12/RC/2278) and Science Foundation Ireland (Grant
42 number 09/IN.1/602).
43
44
45

46 47 REFERENCES

- 48 1. Segalman, R. A., Patterning with block copolymer thin films. *Materials Science &*
49 *Engineering R-Reports* **2005**, *48* (6), 191-226.
- 50 2. Mokarian-Tabari, P.; Vallejo-Giraldo, C.; Fernandez-Yague, M.; Cummins, C.;
51 Morris, M. A.; Biggs, M. J. P., Nanoscale neuroelectrode modification via sub-20 nm silicon
52 nanowires through self-assembly of block copolymers. *Journal of Materials Science-*
53 *Materials in Medicine* **2015**, *26* (2).
- 54 3. Phillip, W. A.; O'Neill, B.; Rodwogin, M.; Hillmyer, M. A.; Cussler, E. L., Self-
55 Assembled Block Copolymer Thin Films as Water Filtration Membranes. *ACS Applied*
56 *Materials & Interfaces* **2010**, *2* (3), 847-853.
57
58
59
60

4. Yin, J.; Yao, X.; Liou, J.-Y.; Sun, W.; Sun, Y.-S.; Wang, Y., Membranes with Highly Ordered Straight Nanopores by Selective Swelling of Fast Perpendicularly Aligned Block Copolymers. *ACS Nano* **2013**, *7* (11), 9961-9974.
5. Xiao, S. G.; Yang, X. M.; Edwards, E. W.; La, Y. H.; Nealey, P. F., Graphoepitaxy of cylinder-forming block copolymers for use as templates to pattern magnetic metal dot arrays. *Nanotechnology* **2005**, *16* (7), S324-S329.
6. Ross, C. A.; Jung, Y. S.; Chuang, V. P.; Son, J. G.; Gotrik, K. W.; Mickiewicz, R. A.; Yang, J. K. W.; Chang, J. B.; Berggren, K. K.; Gwyther, J.; Manners, I. In *Templated self-assembly of Si-containing block copolymers for nanoscale device fabrication*, Proceedings of SPIE - The International Society for Optical Engineering, Engineering, P. o. S.-T. I. S. f. O., Ed. 2010; pp 7637, 76370H.
7. Frascaroli, J.; Brivio, S.; Ferrarese Lupi, F.; Seguini, G.; Boarino, L.; Perego, M.; Spiga, S., Resistive Switching in High-Density Nanodevices Fabricated by Block Copolymer Self-Assembly. *ACS Nano* **2015**, *9* (3), 2518-2529.
8. Crossland, E. J. W.; Kamperman, M.; Nedelcu, M.; Ducati, C.; Wiesner, U.; Smilgies, D. M.; Toombes, G. E. S.; Hillmyer, M. A.; Ludwigs, S.; Steiner, U.; Snaith, H. J., A Bicontinuous Double Gyroid Hybrid Solar Cell. *Nano Letters* **2008**, *9* (8), 2807-2812.
9. Mulherin, R. C.; Jung, S.; Huettner, S.; Johnson, K.; Kohn, P.; Sommer, M.; Allard, S.; Scherf, U.; Greenham, N. C., Ternary Photovoltaic Blends Incorporating an All-Conjugated Donor-Acceptor Diblock Copolymer. *Nano Letters* **2011**, *11* (11), 4846-4851.
10. Bang, J.; Jeong, U.; Ryu, D. Y.; Russell, T. P.; Hawker, C., Block copolymer nanolithography: Translation of molecular level control to nanoscale patterns. *Advanced Materials* **2009**, *21* (47), 4769-4792.
11. Morris, M. A., Directed self-assembly of block copolymers for nanocircuitry fabrication. *Microelectronic Engineering* **2015**, *132*, 207-217.
12. Han, E.; Kang, H.; Liu, C.-C.; Nealey, P. F.; Gopalan, P., Graphoepitaxial Assembly of Symmetric Block Copolymers on Weakly Preferential Substrates. *Advanced Materials* **2010**, *22* (38), 4325-4329.
13. Farrell, R. A.; Kinahan, N. T.; Hansel, S.; Stuen, K. O.; Petkov, N.; Shaw, M. T.; West, L. E.; Djara, V.; Dunne, R. J.; Varona, O. G.; Gleeson, P. G.; Jung, S. J.; Kim, H. Y.; Kolešnik, M. M.; Lutz, T.; Murray, C. P.; Holmes, J. D.; Nealey, P. F.; Duesberg, G. S.; Krstić, V.; Morris, M. A., Large-scale parallel arrays of silicon nanowires via block copolymer directed self-assembly. *Nanoscale* **2012**, *4* (10), 3228-3236.
14. Moon, H.-S.; Shin, D. O.; Kim, B. H.; Jin, H. M.; Lee, S.; Lee, M. G.; Kim, S. O., Large-area, highly oriented lamellar block copolymer nanopatterning directed by graphoepitaxially assembled cylinder nanopatterns. *Journal of Materials Chemistry* **2012**, *22* (13), 6307-6310.
15. Girardot, C.; Böhme, S.; Archambault, S.; Salaün, M.; Latu-Romain, E.; Cunge, G.; Joubert, O.; Zelsmann, M., Pulsed Transfer Etching of PS-PDMS Block Copolymers Self-Assembled in 193 nm Lithography Stacks. *ACS Applied Materials & Interfaces* **2014**, *6* (18), 16276-16282.
16. Cummins, C.; Gangnaik, A.; Kelly, R. A.; Borah, D.; O'Connell, J.; Petkov, N.; Georgiev, Y. M.; Holmes, J. D.; Morris, M. A., Aligned silicon nanofins via the directed self-assembly of PS-*b*-P4VP block copolymer and metal oxide enhanced pattern transfer. *Nanoscale* **2015**, *7* (15), 6712-6721.
17. Kim, S. O.; Solak, H. H.; Stoykovich, M. P.; Ferrier, N. J.; de Pablo, J. J.; Nealey, P. F., Epitaxial self-assembly of block copolymers on lithographically defined nanopatterned substrates. *Nature* **2003**, *424* (6947), 411-414.
18. Delgadillo, P. A. R.; Gronheid, R.; Thode, C. J.; Wu, H.; Cao, Y.; Neisser, M.; Somervell, M.; Nafus, K.; Nealey, P. F., Implementation of a chemo-epitaxy flow for

1
2
3 directed self-assembly on 300-mm wafer processing equipment. *MOEMS* **2012**, *11* (3),
4 031302-1-031302-5.

5 19. Sinturel, C.; Bates, F. S.; Hillmyer, M. A., High χ -Low N Block Polymers: How Far
6 Can We Go? *ACS Macro Letters* **2015**, *4* (9), 1044-1050.

7 20. Bates, C. M.; Seshimo, T.; Maher, M. J.; Durand, W. J.; Cushen, J. D.; Dean, L. M.;
8 Blachut, G.; Ellison, C. J.; Willson, C. G., Polarity-Switching Top Coats Enable Orientation
9 of Sub-10-nm Block Copolymer Domains. *Science* **2012**, *338* (6108), 775-779.

10 21. Cushen, J. D.; Otsuka, I.; Bates, C. M.; Halila, S.; Fort, S.; Rochas, C.; Easley, J. A.;
11 Rausch, E. L.; Thio, A.; Borsali, R.; Willson, C. G.; Ellison, C. J., Oligosaccharide/Silicon-
12 Containing Block Copolymers with 5 nm Features for Lithographic Applications. *ACS Nano*
13 **2012**, *6* (4), 3424-3433.

14 22. Cushen, J. D.; Bates, C. M.; Rausch, E. L.; Dean, L. M.; Zhou, S. X.; Willson, C. G.;
15 Ellison, C. J., Thin Film Self-Assembly of Poly(trimethylsilylstyrene-*b*-*d,l*-lactide) with Sub-
16 10 nm Domains. *Macromolecules* **2012**, *45* (21), 8722-8728.

17 23. Pitet, L. M.; Wuister, S. F.; Peeters, E.; Kramer, E. J.; Hawker, C. J.; Meijer, E. W.,
18 Well-Organized Dense Arrays of Nanodomains in Thin Films of Poly(dimethylsiloxane)-*b*-
19 poly(lactide) Diblock Copolymers. *Macromolecules* **2013**, *46* (20), 8289-8295.

20 24. Cushen, J. D.; Wan, L.; Pandav, G.; Mitra, I.; Stein, G. E.; Ganesan, V.; Ruiz, R.;
21 Grant Willson, C.; Ellison, C. J., Ordering poly(trimethylsilyl styrene-*block-D,L*-lactide)
22 block copolymers in thin films by solvent annealing using a mixture of domain-selective
23 solvents. *Journal of Polymer Science Part B: Polymer Physics* **2014**, *52* (1), 36-45.

24 25. Schulze, M. W.; Sinturel, C.; Hillmyer, M. A., Poly(cyclohexylethylene)-block-
25 poly(ethylene oxide) Block Polymers for Metal Oxide Templating. *ACS Macro Letters* **2015**,
26 *4* (9), 1027-1032.

27 26. Angelescu, D. E.; Waller, J. H.; Adamson, D. H.; Deshpande, P.; Chou, S. Y.;
28 Register, R. A.; Chaikin, P. M., Macroscopic Orientation of Block Copolymer Cylinders in
29 Single-Layer Films by Shearing. *Advanced Materials* **2004**, *16* (19), 1736-1740.

30 27. Gopinadhan, M.; Deshmukh, P.; Choo, Y.; Majewski, P. W.; Bakajin, O.; Elimelech,
31 M.; Kasi, R. M.; Osuji, C. O., Thermally Switchable Aligned Nanopores by Magnetic-Field
32 Directed Self-Assembly of Block Copolymers. *Advanced Materials* **2014**, *26* (30), 5148-
33 5154.

34 28. Ryu, D. Y.; Ham, S.; Kim, E.; Jeong, U.; Hawker, C. J.; Russell, T. P., Cylindrical
35 microdomain orientation of PS-*b*-PMMA on the balanced interfacial interactions:
36 Composition effect of block copolymers. *Macromolecules* **2009**, *42* (13), 4902-4906.

37 29. Zhang, X.; Harris, K. D.; Wu, N. L. Y.; Murphy, J. N.; Buriak, J. M., Fast Assembly
38 of Ordered Block Copolymer Nanostructures through Microwave Annealing. *ACS Nano*
39 **2010**, *4* (11), 7021-7029.

40 30. Zhang, X.; Murphy, J. N.; Wu, N. L. Y.; Harris, K. D.; Buriak, J. M., Rapid Assembly
41 of Nanolines with Precisely Controlled Spacing from Binary Blends of Block Copolymers.
42 *Macromolecules* **2011**, *44* (24), 9752-9757.

43 31. Borah, D.; Shaw, M. T.; Holmes, J. D.; Morris, M. A., Sub-10 nm Feature Size PS-*b*-
44 PDMS Block Copolymer Structures Fabricated by a Microwave-Assisted Solvothermal
45 Process. *ACS Applied Materials & Interfaces* **2013**, *5* (6), 2004-2012.

46 32. Mokarian-Tabari, P.; Cummins, C.; Rasappa, S.; Simao, C.; Sotomayor Torres, C. M.;
47 Holmes, J. D.; Morris, M. A., Study of the Kinetics and Mechanism of Rapid Self-Assembly
48 in Block Copolymer Thin Films during Solvo-Microwave Annealing. *Langmuir* **2014**, *30*
49 (35), 10728-10739.

50 33. Sinturel, C.; Vayer, M.; Morris, M.; Hillmyer, M. A., Solvent Vapor Annealing of
51 Block Polymer Thin Films. *Macromolecules* **2013**, *46* (14), 5399-5415.

- 1
2
3 34. Gotrik, K. W.; Ross, C. A., Solvothermal Annealing of Block Copolymer Thin Films. *Nano Letters* **2013**, *13* (11), 5117-5122.
- 4 35. Gu, X.; Gunkel, I.; Hexemer, A.; Gu, W.; Russell, T. P., An In Situ Grazing Incidence
5 X-Ray Scattering Study of Block Copolymer Thin Films During Solvent Vapor Annealing.
6 *Advanced Materials* **2014**, *26* (2), 273-281.
- 7 36. Gu, X.; Gunkel, I.; Hexemer, A.; Russell, T., Solvent vapor annealing of block
8 copolymer thin films: removal of processing history. *Colloid and Polymer Science* **2014**, *292*
9 (8), 1795-1802.
- 10 37. Paik, M. Y.; Bosworth, J. K.; Smilges, D.-M.; Schwartz, E. L.; Andre, X.; Ober, C.
11 K., Reversible Morphology Control in Block Copolymer Films via Solvent Vapor
12 Processing: An in Situ GISAXS Study. *Macromolecules* **2010**, *43* (9), 4253-4260.
- 13 38. Sinturel, C.; Grosso, D.; Boudot, M.; Amenitsch, H.; Hillmyer, M. A.; Pineau, A.;
14 Vayer, M., Structural Transitions in Asymmetric Poly(styrene)-*block*-Poly(lactide) Thin
15 Films Induced by Solvent Vapor Exposure. *ACS Applied Materials & Interfaces* **2014**, *6* (15),
16 12146-12152.
- 17 39. Mokarian-Tabari, P.; Collins, T. W.; Holmes, J. D.; Morris, M. A., Cyclical
18 "Flipping" of Morphology in Block Copolymer Thin Films. *ACS Nano* **2011**, *5* (6), 4617-
19 4623.
- 20 40. Park, W. I.; Tong, S.; Liu, Y.; Jung, I. W.; Roelofs, A.; Hong, S., Tunable and rapid
21 self-assembly of block copolymers using mixed solvent vapors. *Nanoscale* **2014**, *6* (24),
22 15216-15221.
- 23 41. She, M.-S.; Lo, T.-Y.; Ho, R.-M., Controlled Ordering of Block Copolymer Gyroid
24 Thin Films by Solvent Annealing. *Macromolecules* **2013**, *47* (1), 175-182.
- 25 42. Keen, I.; Yu, A.; Cheng, H.-H.; Jack, K. S.; Nicholson, T. M.; Whittaker, A. K.;
26 Blakey, I., Control of the Orientation of Symmetric Poly(styrene)-*block*-poly(d,l-lactide)
27 Block Copolymers Using Statistical Copolymers of Dissimilar Composition. *Langmuir* **2012**,
28 *28* (45), 15876-15888.
- 29 43. Keen, I.; Cheng, H.-H.; Yu, A.; Jack, K. S.; Younkin, T. R.; Leeson, M. J.; Whittaker,
30 A. K.; Blakey, I., Behavior of Lamellar Forming Block Copolymers under Nanoconfinement:
31 Implications for Topography Directed Self-Assembly of Sub-10 nm Structures.
32 *Macromolecules* **2013**, *47* (1), 276-283.
- 33 44. Baruth, A.; Rodwogin, M. D.; Shankar, A.; Erickson, M. J.; Hillmyer, M. A.;
34 Leighton, C., Non-lift-off Block Copolymer Lithography of 25 nm Magnetic Nanodot
35 Arrays. *ACS Applied Materials & Interfaces* **2011**, *3* (9), 3472-3481.
- 36 45. Smilgies, D. M.; Busch, P.; Papadakis, C. M.; Posselt, D., Characterization of
37 polymer thin films with small-angle X-ray scattering under grazing incidence (GISAXS).
38 *Synchrotron Radiation News* **2002**, *15* (5), 35-42.
- 39 46. Stamm, M., Polymer Surface and Interface Characterization Techniques. In *Polymer*
40 *Surfaces and Interfaces*, Stamm, M., Ed. Springer Berlin Heidelberg: 2008; pp 1-16.
- 41 47. Andrezza, P., Probing Nanoalloy Structure and Morphology by X-Ray Scattering
42 Methods. In *Nanoalloys*, Alloyeau, D.; Mottet, C.; Ricolleau, C., Eds. Springer London:
43 2012; pp 69-112.
- 44 48. Müller-Buschbaum, P., Grazing incidence small-angle X-ray scattering: an advanced
45 scattering technique for the investigation of nanostructured polymer films. *Analytical and*
46 *Bioanalytical Chemistry* **2003**, *376* (1), 3-10.
- 47 49. Zhang, J.; Posselt, D.; Smilgies, D.-M.; Perlich, J.; Kyriakos, K.; Jaksch, S.;
48 Papadakis, C. M., Lamellar Diblock Copolymer Thin Films during Solvent Vapor Annealing
49 Studied by GISAXS: Different Behavior of Parallel and Perpendicular Lamellae.
50 *Macromolecules* **2014**, *47* (16), 5711-5718.
- 51
52
53
54
55
56
57
58
59
60

- 1
2
3 50. Maret, M.; Tiron, R.; Chevalier, X.; Gergaud, P.; Gharbi, A.; Lapeyre, C.; Pradelles,
4 J.; Jousseau, V.; Fleury, G.; Hadziioannou, G.; Boudet, N.; Navarro, C., Probing Self-
5 Assembly of Cylindrical Morphology Block Copolymer Using in Situ and ex Situ Grazing
6 Incidence Small-Angle X-ray Scattering: The Attractive Case of Graphoepitaxy.
7 *Macromolecules* **2014**, *47* (20), 7221-7229.
- 8 51. Cummins, C.; Mokarian-Tabari, P.; Holmes, J. D.; Morris, M. A., Selective etching of
9 polylactic acid in poly(styrene)-*block*-poly(d,l)lactide diblock copolymer for nanoscale
10 patterning. *Journal of Applied Polymer Science* **2014**, *131* (18).
- 11 52. McKenna, F. H. a. G. B., Physical Properties of Polymers Handbook. *AIP Press* **1996**,
12 379-400.
- 13 53. Ho, R. M.; Tseng, W. H.; Fan, H. W.; Chiang, Y. W.; Lin, C. C.; Ko, B. T.; Huang, B.
14 H., Solvent-induced microdomain orientation in polystyrene-*b*-poly (L-lactide) diblock
15 copolymer thin films for nanopatterning. *Polymer* **2005**, *46* (22), 9362-9377.
- 16 54. Hou, X.; Li, Q.; Cao, A., Solvent annealing-induced microphase-separation of
17 polystyrene-*b*-polylactide block copolymer aimed at preparation of ordered
18 nanoparticles/block copolymer hybrid thin film. *J Polym Res* **2014**, *21* (7), 1-15.
- 19 55. Vayer, M.; Hillmyer, M. A.; Dirany, M.; Thevenin, G.; Erre, R.; Sinturel, C.,
20 Perpendicular orientation of cylindrical domains upon solvent annealing thin films of
21 polystyrene-*b*-polylactide. *Thin Solid Films* **2010**, *518* (14), 3710-3715.
- 22 56. Hong, S. W.; Gu, W.; Huh, J.; Sveinbjornsson, B. R.; Jeong, G.; Grubbs, R. H.;
23 Russell, T. P., On the Self-Assembly of Brush Block Copolymers in Thin Films. *ACS Nano*
24 **2013**, *7* (11), 9684-9692.
- 25 57. Busch, P.; Rauscher, M.; Smilgies, D.-M.; Posselt, D.; Papadakis, C. M., Grazing-
26 incidence small-angle X-ray scattering from thin polymer films with lamellar structures - the
27 scattering cross section in the distorted-wave Born approximation. *Journal of Applied*
28 *Crystallography* **2006**, *39* (3), 433-442.
- 29 58. Yoon, J.; Yang, S. Y.; Lee, B.; Joo, W.; Heo, K.; Kim, J. K.; Ree, M., Nondestructive
30 quantitative synchrotron grazing incidence X-ray scattering analysis of cylindrical
31 nanostructures in supported thin films. *Journal of Applied Crystallography* **2007**, *40* (2), 305-
32 312.
- 33 59. Borah, D.; Simao, C. D.; Senthamaraiannan, R.; Rasappa, S.; Francone, A.; Lorret,
34 O.; Salaun, M.; Kosmala, B.; Kehagias, N.; Zelsmann, M.; Sotomayor-Torres, C. M.; Morris,
35 M. A., Soft-graphoepitaxy using nanoimprinted polyhedral oligomeric silsesquioxane
36 substrates for the directed self-assembly of PS-*b*-PDMS. *European Polymer Journal* **2013**, *49*
37 (11), 3512-3521.
- 38 60. Jung, Y. S.; Ross, C. A., Orientation-Controlled Self-Assembled Nanolithography
39 Using a Polystyrene-Polydimethylsiloxane Block Copolymer. *Nano Letters* **2007**, *7* (7),
40 2046-2050.
- 41 61. Jeong, S.-J.; Moon, H.-S.; Shin, J.; Kim, B. H.; Shin, D. O.; Kim, J. Y.; Lee, Y.-H.;
42 Kim, J. U.; Kim, S. O., One-Dimensional Metal Nanowire Assembly via Block Copolymer
43 Soft Graphoepitaxy. *Nano Letters* **2010**, *10* (9), 3500-3505.
- 44 62. Pickett, G. T.; Witten, T. A.; Nagel, S. R., Equilibrium surface orientation of lamellae.
45 *Macromolecules* **1993**, *26* (12), 3194-3199.
- 46 63. Borah, D.; Rassapa, S.; Shaw, M. T.; Hobbs, R. G.; Petkov, N.; Schmidt, M.; Holmes,
47 J. D.; Morris, M. A., Directed self-assembly of PS-*b*-PMMA block copolymer using HSQ
48 lines for translational alignment. *Journal of Materials Chemistry C* **2013**, *1* (6), 1192-1196.
- 49 64. Zalusky, A. S.; Olayo-Valles, R.; Wolf, J. H.; Hillmyer, M. A., Ordered Nanoporous
50 Polymers from Polystyrene-Polylactide Block Copolymers. *Journal of the American*
51 *Chemical Society* **2002**, *124* (43), 12761-12773.
- 52
53
54
55
56
57
58
59
60

- 1
2
3 65. Koo, K.; Ahn, H.; Kim, S.-W.; Ryu, D. Y.; Russell, T. P., Directed self-assembly of
4 block copolymers in the extreme: guiding microdomains from the small to the large. *Soft*
5 *Matter* **2013**, *9* (38), 9059-9071.
6 66. Ivan Wichterle, J. L., Antoine Vapor Pressure Constants of Pure Compounds.
7 *Academia* **1971**.
8 67. Olayo-Valles, R.; Guo, S. W.; Lund, M. S.; Leighton, C.; Hillmyer, M. A.,
9 Perpendicular domain orientation in thin films of polystyrene - Polylactide diblock
10 copolymers. *Macromolecules* **2005**, *38* (24), 10101-10108.
11
12
13
14
15
16
17
18
19
20
21
22
23
24
25
26
27
28
29
30
31
32
33
34
35
36
37
38
39

40 **Figures (1-6) and tables (1-3)**

41 **Solvo-thermal vapor annealing of lamellar poly(styrene)-*block*-poly(D,L-**
42 **lactide) block copolymer thin films for directed self-assembly application**
43
44
45
46
47
48
49
50
51
52
53
54
55
56
57
58
59
60

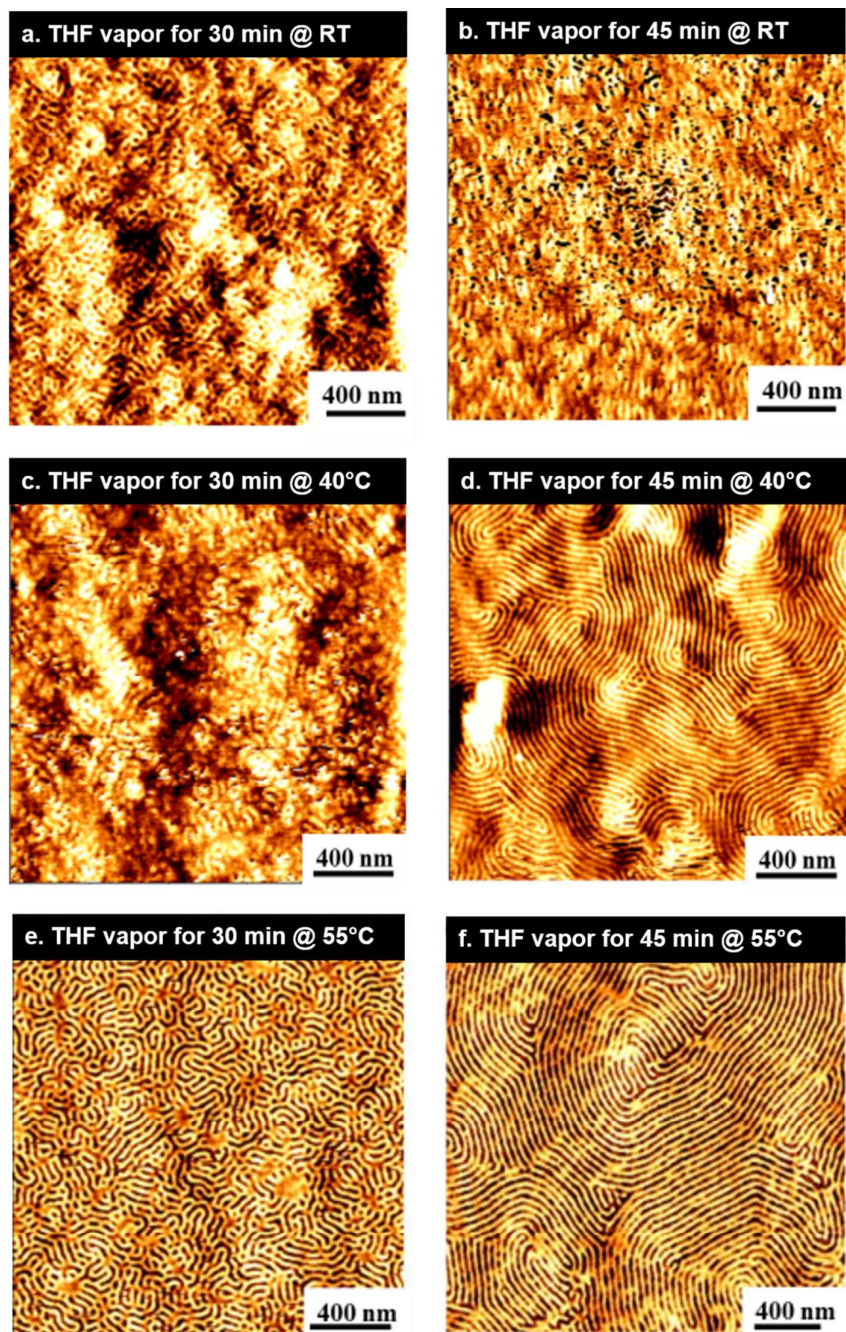


Figure 1. PS-*b*-PLA pattern formation after solvo-thermal vapor annealing (STVA) at different temperatures. Atomic force microscope topographic images of 0.5 wt % PS-*b*-PLA thin films on silicon after (a) 30 min SVA with THF at room temperature, (b) 45 min SVA with THF at room temperature, (c) 30 min STVA with THF @ 40°C, (d) 45 min STVA with THF @ 40°C, (e) 30 min STVA with THF @ 55°C, (f) 45 min STVA with THF @ 55°C.

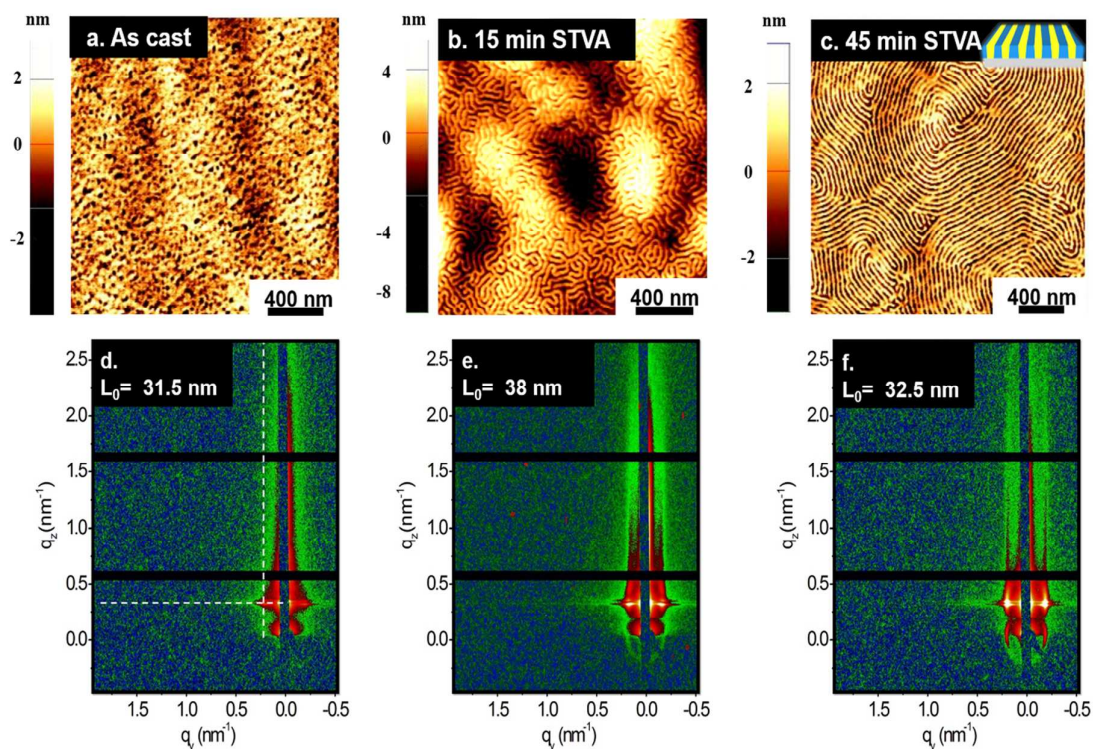


Figure 2. Evolution of PS-*b*-PLA pattern with solvo-thermal vapor anneal treatment. Atomic force microscope topographic images of PS-*b*-PLA BCP films (a) as-cast and after solvo-thermal vapor anneal with THF @ 55°C as shown in (b) 15 and (c) 45 min. (d-f) Corresponding GISAXS patterns for (a) – (c) with L_0 value (repeat periodicity) calculated from GISAXS measurements. The white dashed lines in the d) pattern correspond to the 1D cut positions.

Table 1. Polymer-solvent (P-S) interaction parameter (χ_{P-S}) for PS-*b*-PLA and THF and CHCl_3 solvent.

T(°C)	$\chi_{\text{PS-THF}}$	$\chi_{\text{PLA-THF}}$	$\chi_{\text{PS-CHCl}_3}$	$\chi_{\text{PLA-CHCl}_3}$
23°C	0.35	0.60	0.34	0.68
40°C	0.35	0.59	0.34	0.64
55°C	0.35	0.57	0.34	0.62

Table 2. Contact angle of silicon after different treatment techniques and film thickness of PS-*b*-PLA BCP material after casting and solvo-thermal vapor annealing in THF vapors at 55°C.

Substrate treatment	Contact angle	As cast film thickness on treated substrate (± 0.5 nm)	Thickness after SVA for 45 min on treated substrate (± 0.5 nm)
Piranha cleaned Si + chloroform sonication	$\sim 25^\circ$	47.0 nm	48.9 nm
HMDS treated Si	$\sim 70^\circ$	47.8 nm	48.0 nm

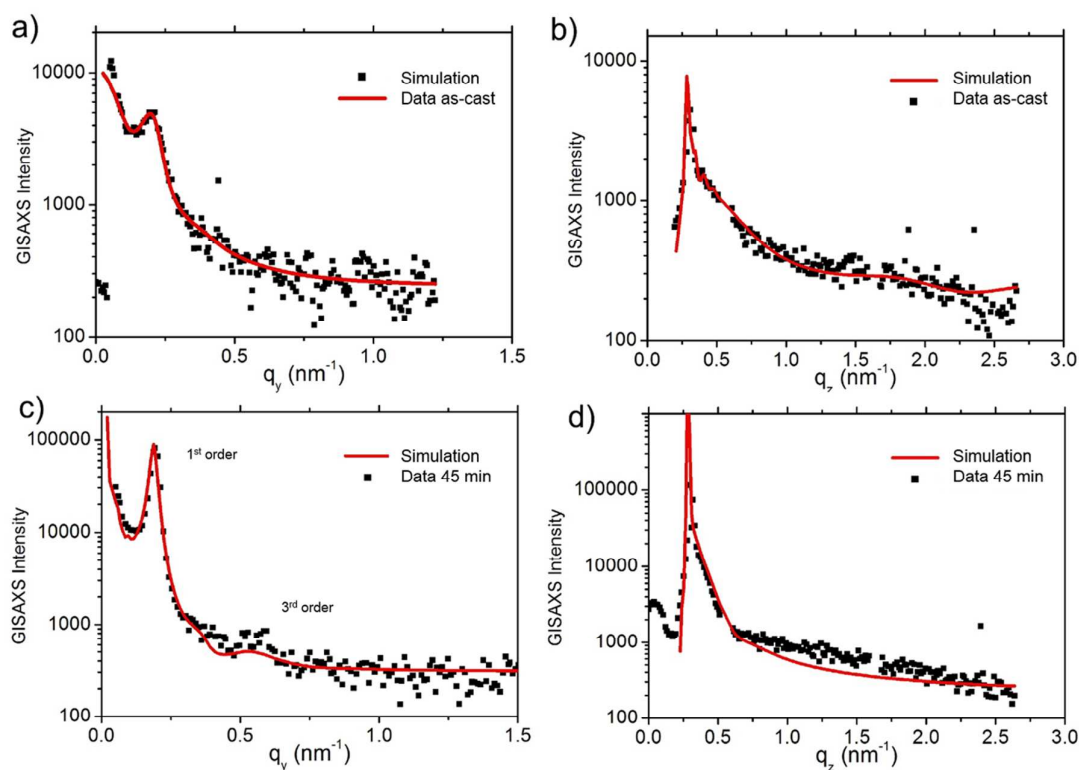


Figure 3. GISAXS experimental (black squares) and simulated (red line) curves for the samples (a,b) as-cast and after solvo-thermal vapor annealing with THF @ 55°C after (c,d) 45 minutes. The q_y (resp. q_z) horizontal (resp. vertical) cross sections are extracted from the GISAXS patterns in Figure 2 and best fits obtained with IsGISAXS software (red line).

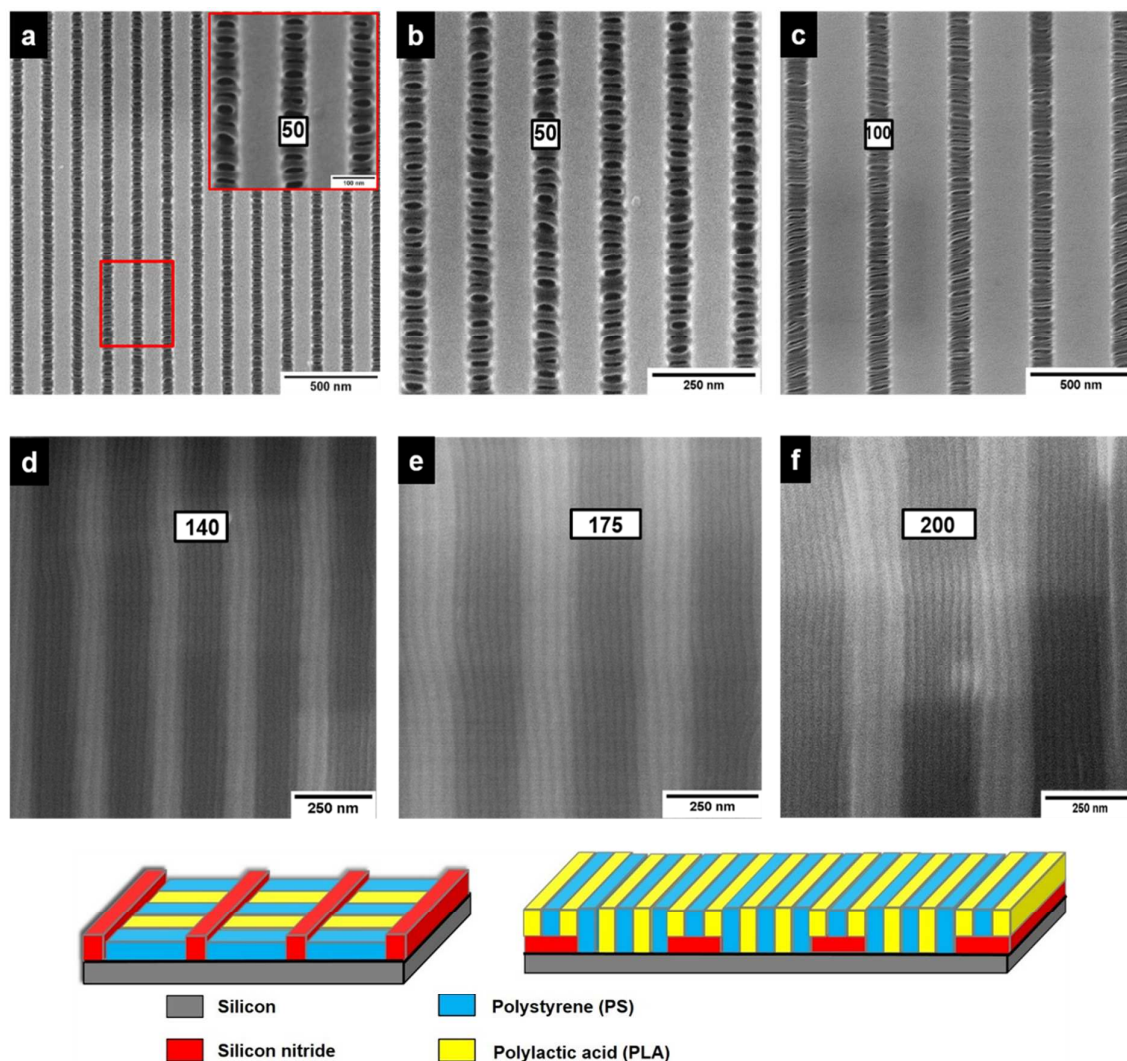


Figure 4. Directed self-assembly of PS-*b*-PLA thin films on Si₃N₄ patterned substrates. (a-c) Top-down SEM images of PS-*b*-PLA self-assembly with perpendicular alignment of domains to Si₃N₄ sidewalls after STVA with THF @ 55°C. Darker areas represent the channels and bright areas are the mesas. (d-f) Top-down SEM images showing directed assembly of PS-*b*-PLA films after STVA with THF @ 55°C with domain alignment parallel to sidewalls. Si₃N₄ channel widths are marked in respective images. Films were stained with RuO₄ vapors to enhance contrast. PS domains appear dark and PLA domains are bright. Both possible alignments are represented schematically.

Table 3. Characteristics of PS-*b*-PLA block copolymer used in this study.

Block Copolymer	Molecular Weight (kg mol ⁻¹)	Pitch - AFM	Pitch - GISAXS	χ @ 23°C	χ @ 40°C	χ @ 55°C
PS- <i>b</i> -PLA	21-19.5	~33.7 nm	~32.5 nm	~ 0.219	~ 0.201	~ 0.187

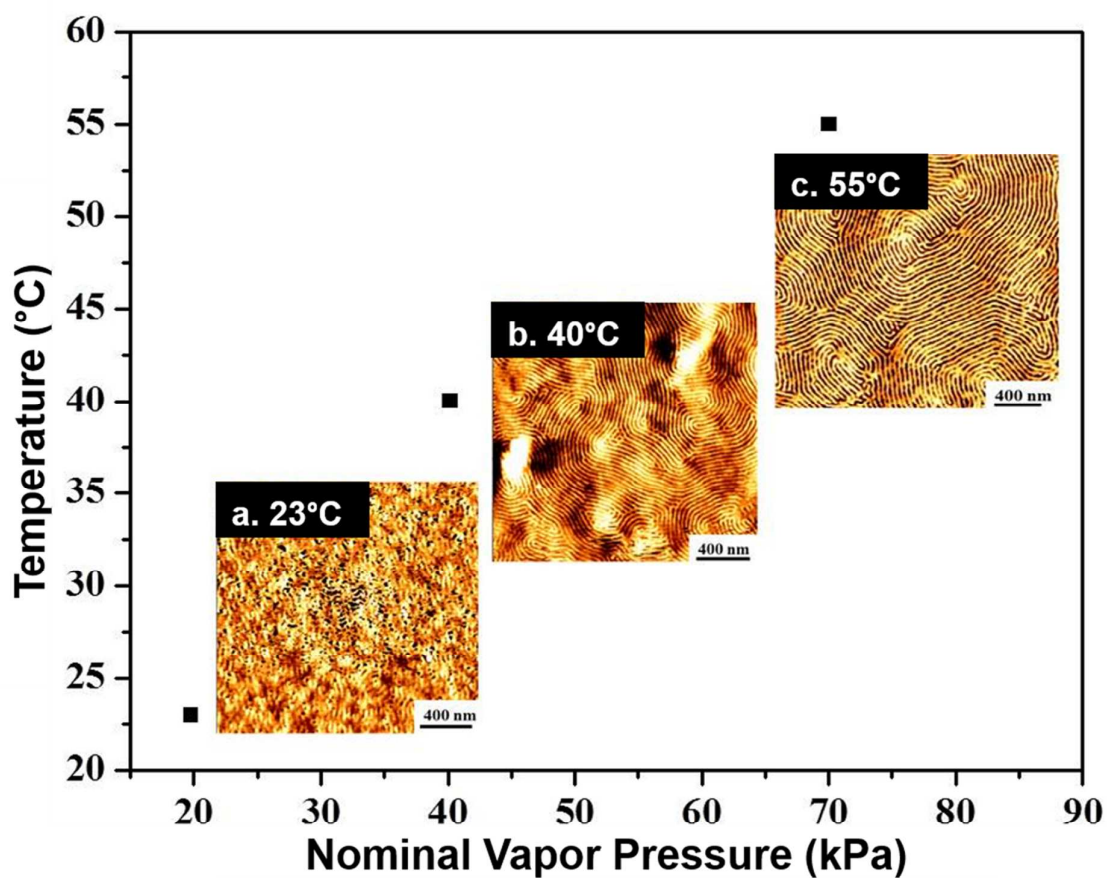


Figure 5. Graph reflecting correlation of THF nominal vapor pressure with increasing temperature. PS-*b*-PLA self-assembly was induced via increasing THF vapor pressure with increased temperature. Insets (b) and (c) shows highly ordered PS-*b*-PLA domains after SVA with THF @ 40°C and 55°C respectively, while (a) shows no microphase separation was observed at room temperature (*i.e.* 23°C).

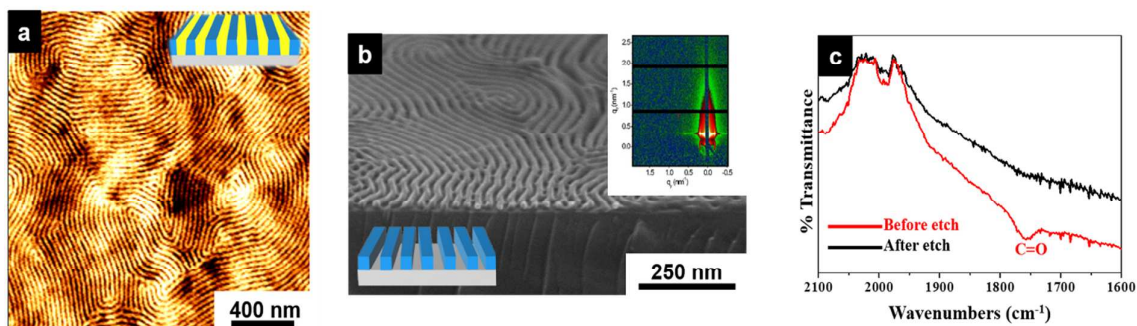


Figure 6. (a) AFM image of thin film of PS-*b*-PLA self-assembly on HMDS functionalized silicon following 45 minutes STVA. (b) Cross-section SEM of etched PS-*b*-PLA film following 5 minute immersion of film in 0.01 M NaOH solution. Inset in (b) shows corresponding GISAXS pattern retaining the same order as the initial self-assembled film. (c) FT-IR data of film before and after etch treatment showing removal of PLA component. (a) and (b) scale bars represent 250 nm.

For Table of Contents Use;

